

# Electromagnetic Field Analysis and Motor Testing for the Development of Application Technology of Electrical Steel Sheets

Kiyoshi WAJIMA\*  
Yasuo OHSUGI

Ryu HIRAYAMA

## Abstract

*Non-oriented electrical steel (NO) is widely used for motor cores since it economically meets the requirements for size reduction and efficiency improvement of motors. The demand for global environmental protection and economical use of energy has promoted developments of new NO products with improved properties. In order to fully utilize the superior characteristics of such products, the application technology is also important. In this paper, we introduce examples of iron loss analysis methods and motor testing as the basis of application technology development.*

## 1. Introduction

Non-oriented electrical steel (hereinafter referred to as NO) is widely used for motor cores and new NO materials have been developed to meet the demand for high performance motors, such as traction motors of hybrid/electric vehicles or compressor motors of air conditioners. Improved magnetization characteristics and lower iron loss are firstly demanded as the iron core material. The characteristics of NO are influenced by alloy compositions, grain size and orientation, steel material purity and internal stress. However, these factors exert adverse effects on the magnetization characteristics and iron loss. Therefore, high performance NO materials have been realized by steadily controlling these metallurgical approaches to achieve target properties.

In order to further enhance the performance of motors using the superior characteristics of such high performance, non-oriented electrical steel, application technology that reduces the influence of various building factors (deteriorating factors) in the actual condition of motor cores is also important. The building factors of iron loss of motor cores are as follows: (1) Magnetic flux distribution, (2) Rotational magnetic flux, (3) Time harmonics, (4) Spatial harmonics, (5) DC-biased magnetic flux, (6) Mechanical stress, (7) Inter-layer short and (8) Temperature. Therefore, it is crucial for the application technology of electrical steel to breakdown and clarify the generating factors of motor loss in actual working conditions by using various analysis and evaluation technologies. The study for improving the performance of motors can be realized thereby.

This article introduces the electromagnetic field analysis and the

motor testing technology as the basis of application technology of NO electrical steel. In the second section, this article describes a method that calculates the iron loss of NO electrical steel magnetized by distorted magnetic flux density which includes time harmonics and spatial harmonics with high accuracy and within a practically acceptable calculation time period. The electromagnetic field analysis method for motors has made significant progress in recent years. However, the calculation of motor performance with respect to all building factors taken into consideration requires high calculation expenditure. Therefore, motor measurement testing is necessary to evaluate the final performance of motors with various NO electrical steel core materials. In the third section, an example of the result of the application of the newly developed NO to induction motors is described.

## 2. Iron Loss Analysis Method under Distorted Magnetic Flux (Density) Excitation

In the designing of magnetic circuits of highly efficient motors such as the interior permanent magnet synchronous motor (IPMSM), electromagnetic analysis is indispensable. Non-oriented electrical steel sheets of motor cores are acted upon by the magnetic flux of various harmonics caused by slot harmonics and switching of the inverter power source. Since these harmonics increase motor iron loss, in the study based on motor electromagnetic field analysis technology, improvement of iron loss calculation accuracy under harmonic magnetic flux excitation is an important research subject.

For this purpose appropriate modeling of the characteristics of

\* Chief Researcher, Instrumentation & Control Research Lab., Process Research Laboratories  
20-1 Shintomi, Futtsu City, Chiba Pref. 293-8511

the electrical steel sheet used as a core is important. Particularly, because under the superpositioned magnetic flux of pluralities of harmonics, non-oriented electrical steel sheets exhibit a complicated magnetizing behavior, study should be conducted along with investigation with actual measurement data. In this paper, iron losses of several non-oriented (NO) electrical steel ring cores were measured under pulse width modulation (PWM) voltage excitation that causes typical distorted magnetic flux density waveforms in a stator core of interior permanent magnet (IPM) motors. Iron losses were also computed by several iron loss models and compared with the measured values to evaluate the accuracy of each model.<sup>1)</sup>

**2.1 Measurement method and results**

By using the magnetization characteristic measuring system shown in Fig. 1, the iron loss of a ring core sample was measured. The sample was excited by a magnetic flux density of a waveform consisting of motor spatial harmonics and inverter harmonics. The system enables exciting samples with a voltage of an arbitrary waveform and herein, the waveform shown in Fig. 2, known as the benchmark Model D of the Institute of Electrical Engineers of Japan, was selected as an example for application to the stator core of an interior permanent magnet synchronous motor (IPMSM). By exciting the ring core sample with the waveform voltage, which is

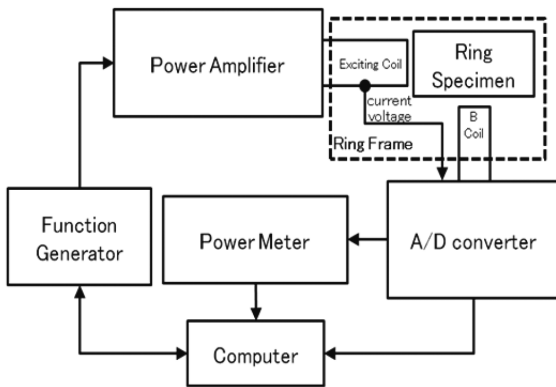


Fig. 1 Diagram of measurement system of ring core excited by PWM voltage waveforms which causes arbitrary magnetic flux density B waveforms

equivalent to the magnetic flux waveform, the influence of the motor harmonics was considered. Inverter voltage waveforms are decided based on single phase PWM switching logic under fixed DC voltage input so that it causes the target distorted magnetic flux density waveform in the ring core. Thus, it is possible to measure iron losses under the influence of various harmonics.

Figure 3 shows the hysteresis loops of a ring core sample (external diameter 47 mm, internal diameter 33 mm, core thickness 7 mm) of JIS 35A300 excited by a distorted waveform and the PWM voltage (modulation index  $m=1.0$  and  $0.4$ , respectively) with a carrier frequency of 5 kHz. It is observed from the figure that as the excitation waveform shifts from the distorted waveform to the PWM waveform of the modulation index 0.4 having a higher rate of harmonics, the width of the hysteresis loop grows larger and the iron loss increases. Since this is a typical change of hysteresis loops affected by eddy current, it is presumed that eddy current induced by high frequency from PWM waveforms is a primary factor of the iron loss increment. As the magnetic flux density waveforms used for the measurement include various frequency components, the measured iron losses cannot be separated into the hysteresis loss and eddy current loss by the two frequency methods as shown in the reference<sup>2)</sup>. However, another research<sup>3)</sup> states that under sinusoidal PWM inverter excitation, the influence of minor loops that increase hysteresis loss is small. Therefore, it is considered that the application of the iron loss calculation model with accurate eddy current calculation is effective for improving the iron loss calculation accuracy under distorted magnetic flux excitation.

**2.2 Iron loss calculation models and their evaluation results**

Three types of iron loss calculation models,<sup>4-6)</sup> each having a different eddy current model, were applied to the electromagnetic simulation of ring core models and the calculation results were compared with the measured iron loss values to evaluate their accuracies. The ring cores are constructed from laminated NO electrical steel sheets of JIS 35A210, 35A300, 50A470 and 50A1300, respectively.

The following iron loss calculation models were used to evaluate accuracy.

(a) Model-A: The magnetic flux density waveform  $B$  of each finite element mesh is calculated by two dimensional electromagnetic field analysis. Then the hysteresis loss  $W_h$  is calculated by Formula

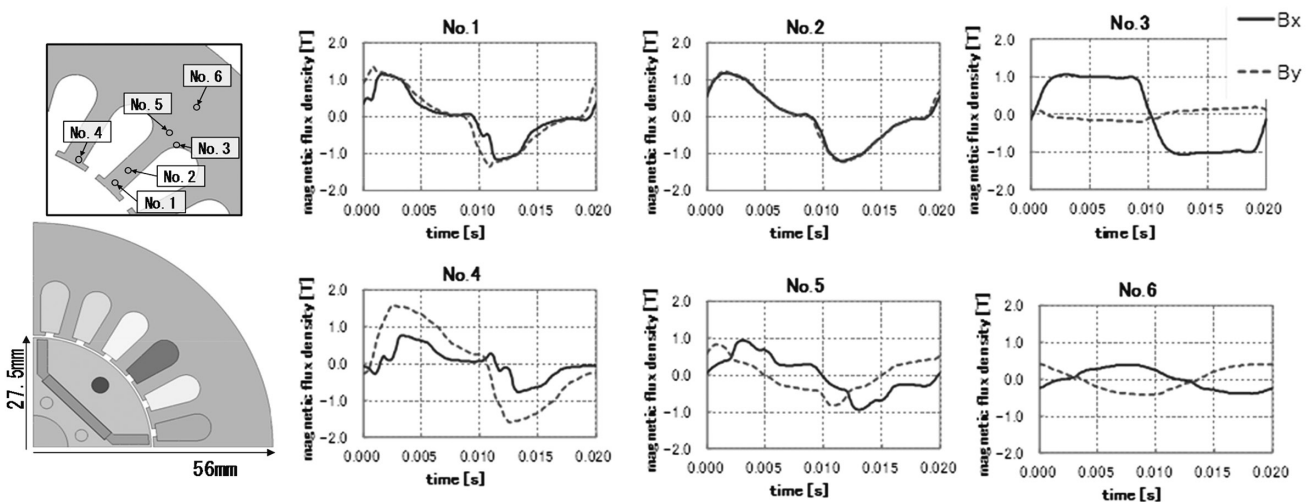


Fig. 2 Distorted magnetic flux density B waveforms in the stator core of the IPM motor estimated by FEM

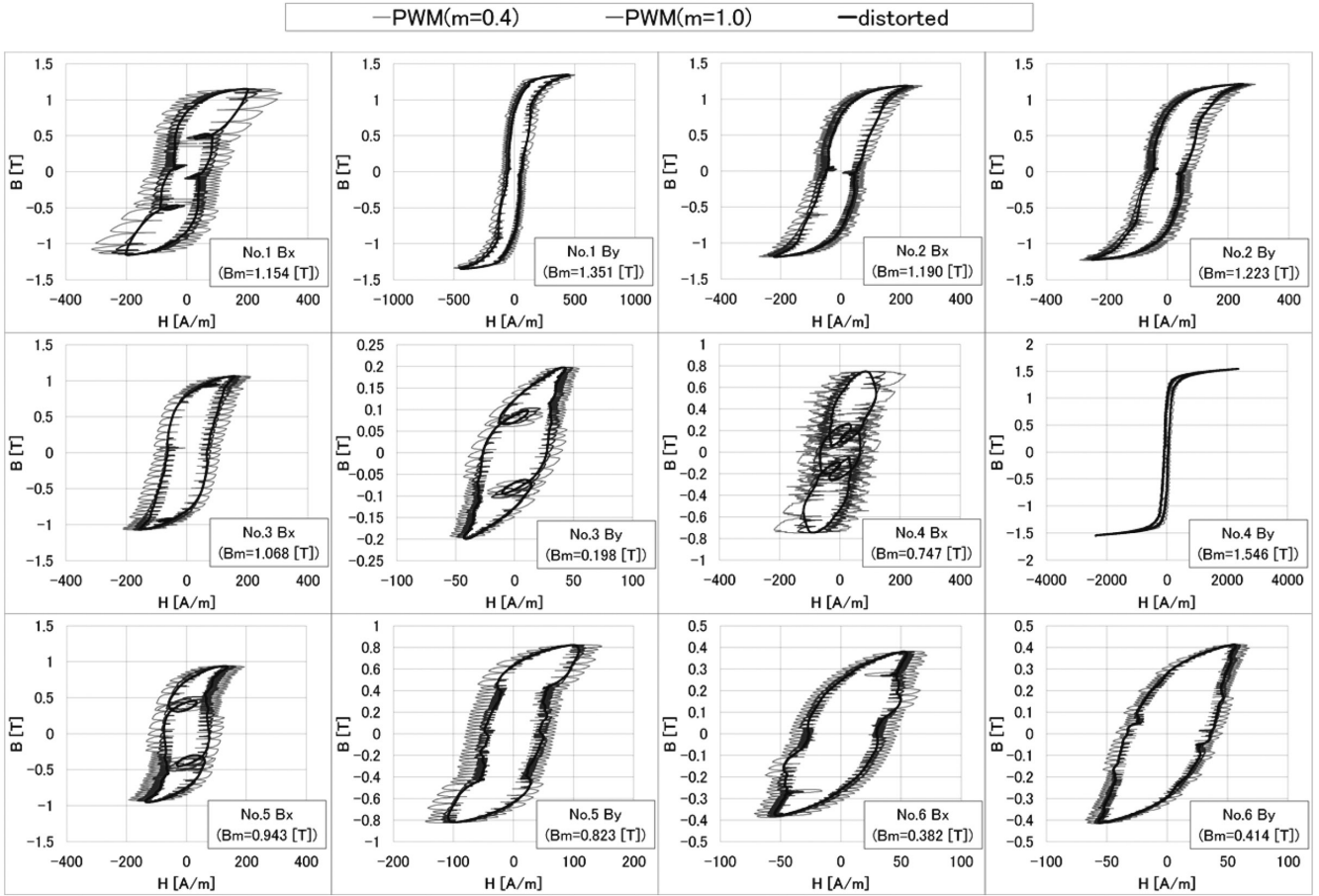


Fig. 3 Hysteresis loops of 35A300 excited by distorted B waveform and PWM voltage (m=1.0 and 0.4)

(1) and the eddy current loss  $W_e$  is calculated by Formula (2).<sup>4)</sup> In the calculation using other iron loss models, Formula (1) was used commonly for hysteresis  $W_h$ .

$$W_h = \frac{K_h}{T} \sum_{j=1}^N B p_j^{1.6} \quad (1)$$

$$W_e = \frac{K_e}{2\pi} \frac{1}{T} \int_0^T \left| \frac{dB}{dt} \right|^2 dt \quad (2)$$

Where  $K_h$ ,  $K_e$  are Steinmetz coefficients,  $Bp$  is the magnetic flux density amplitudes of the major loop and the minor loop, and  $T$  is the fundamental cycle. This iron loss model is very basic and it is based on the assumption that the eddy current in the electrical steel sheet distributes uniformly in the direction of the thickness. Therefore, this model does not take the skin effect of eddy current into account.

(b) Model-B: Eddy current and magnetic flux density are obtained by three dimensional electromagnetic field analysis using mesh models divided in the sheet thickness direction. The eddy current loss is calculated by Formula (3).<sup>5)</sup> This model is accurate but requires large computing time.

$$W_e = \kappa W_e' = \kappa \frac{1}{T} \int_0^T \int \frac{J_e^2}{\sigma} dV dt \quad (3)$$

Where  $\kappa$  is the abnormal eddy current loss coefficient and is defined as the ratio of the measured eddy current loss estimated by two frequency methods to the classical eddy current loss. Further,  $\sigma$  is the conductivity of the electrical steel sheet.

(c) Model-C: The distribution of vector potential  $A$  in the sheet thickness direction is calculated by solving the first order Equation (4) under the boundary conditions obtained from the result of Model-A. The eddy current distribution in the electrical steel sheet is calculated by Formula (5).<sup>6)</sup> Eddy current loss is calculated by inserting  $J_e$  obtained by Formula (5) into Formula (3).

$$\frac{\partial}{\partial z} \left( \frac{1}{\mu} \frac{\partial A}{\partial z} \right) = \sigma \frac{\partial A}{\partial t} \quad (4)$$

$$J_e = -\sigma \frac{\partial A}{\partial t} \quad (5)$$

Where  $\mu$  is the magnetic permeability of the electrical steel sheet and assumed to be uniform in the entire sheet thickness direction in the calculation of Equation (4). Since the magnetic permeability under practical inverter excitation is considered to be unevenly distributed to a certain degree in the thickness direction, it is necessary to investigate the influence of the assumption by comparing the calculated values with measured iron loss values.

Figure 4 shows scatter diagrams of iron loss calculated by the respective models vs. the measured values. The case of the inverter with a modulation index of 0.4, which exhibits the highest increase of iron loss, is shown. Among the combinations of various electrical steel sheets and waveforms, it is confirmed that Model-A exhibits relatively large errors and Model-B and Model-C exhibit high accuracy. Measured values and errors of respective iron loss calculation models are arranged and shown in Fig. 5 for the case of excitation by a complicated waveform consisting of minor loops, saturated

waveforms and special motor harmonic components. Model-A overestimates the iron loss values, which shows that the influence of the skin effect of eddy current in the electrical steel sheet in the model should not be disregarded. Model-B maintains thorough high accuracy and verifies that the correct estimation of the behavior of the eddy current within the electrical steel sheet is effective in estimating iron loss with high accuracy. Model-C shows sufficient accuracy for practical use and is considered to be most suitable among the three iron loss models for practical use from the viewpoint of calculation time.

This study confirmed that in the estimation of the iron loss of the cores of inverter-driven motors, the calculation model of eddy current loss of electrical steel sheets is crucial. From the viewpoints of

calculation accuracy and computing time, Model-C that employs two-dimensional static magnetic field analysis in combination with the first order eddy current calculation has the highest practicability among the evaluated three iron loss calculation models.

### 3. Evaluation of Induction Motor Constructed with High Magnetic Flux Density Electrical Steel

It is estimated that the ratio of the electric consumption of motors is about half of the total world consumption and more than half of which is occupied by industrial motors. In this situation, Japan introduced, in April 2015, Top Runner Standards of the IE3 class for three-phase induction motors that are widely used as industrial motors. Since three-phase, squirrel-cage induction motors do not have permanent magnets in their rotors, they have to generate the necessary magnetic flux only by excitation due to the stator's primary winding currents. Therefore, applying high magnetic flux density materials to induction motors is considered to effectively improve efficiency because it enables reduction of the motor current. With such a background, high magnetic flux density NO material shown in Fig. 6 has been developed to contribute to the improvement of efficiency of induction motors.<sup>7)</sup> Compared to the JIS grade material with the same W15/50 value (iron loss under excitation of 1.5 T at 50 Hz)<sup>8)</sup>, the new series materials have 0.02 T to 0.05 T higher B50 values (the magnetic flux density under a magnetizing force of 5000 A/m). These high magnetic induction properties achieve a higher magnetic flux density with the same excitation current. To confirm the effect of applying the newly developed NO material to induction motors, the stator cores of different NO material were made and the efficiency of each induction motor was tested with the motor testing system.<sup>9)</sup>

#### 3.1 Testing system and testing method

Table 1 shows the specification of the tested motor. It was a three-phase, squirrel-cage induction motor and the squirrel-cage secondary conductor was made of aluminum with the end ring and rotor bar brazed and bonded to each other. The rotor core was made of 50H-CH shown in Fig. 6. As for the stator, three types were pre-

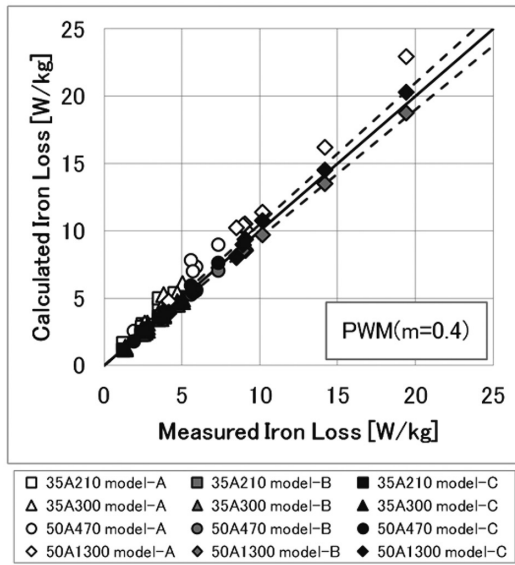


Fig. 4 Measured and calculated iron losses excited by PWM voltage waveform (m=0.4)

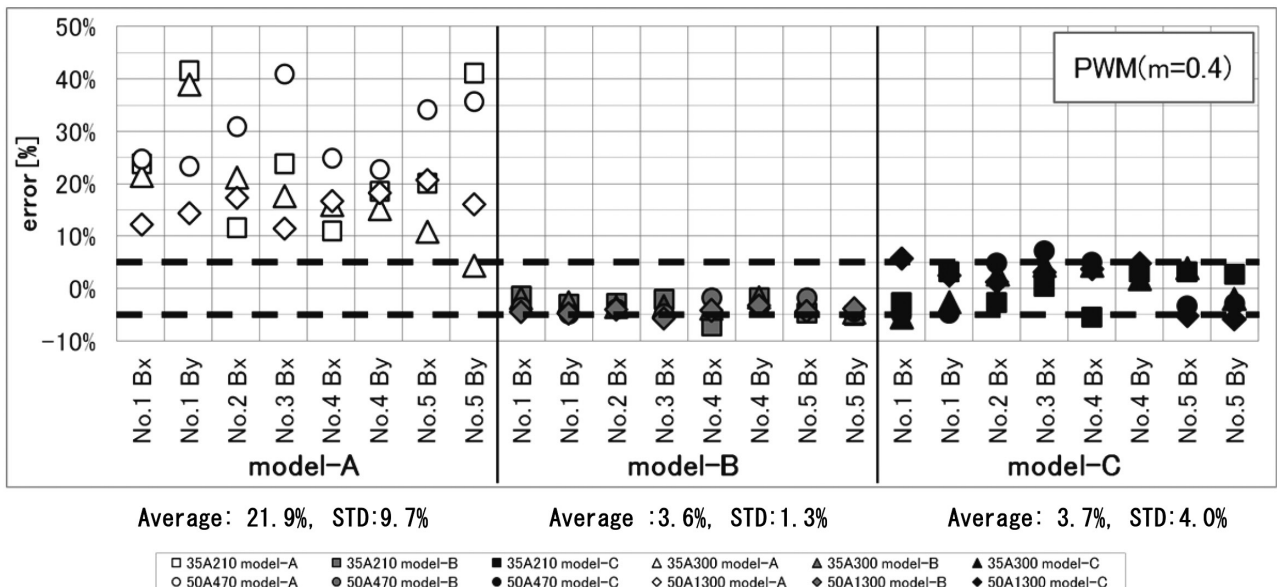
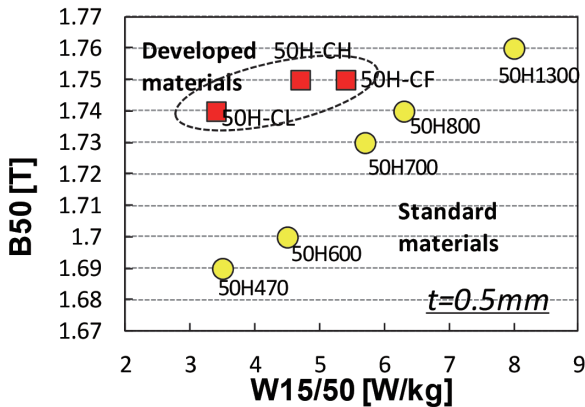


Fig. 5 Calculation errors of each iron loss model Iron losses excited by PWM voltage waveform (m=0.4).

pared for testing: the newly developed 50H-CL, 50H-CH and JIS grade 50H470 as a reference. The material properties of core materials actually used in the tested motors are shown in **Table 2**.

**Figure 7** shows the configuration of the test equipment. A three-phase alternating current was provided from an inverter to the test motor to drive it. The rotation speed and torque to calculate the motor output were measured with a torque meter. Input current and voltage to the test motor were measured and the data was sent to a power meter to obtain input power from the inverter. A thermocouple was set on the stator winding of each test motor to measure the



**Fig. 6** Iron loss and magnetic flux density of the newly developed non-oriented electrical steel sheets and the conventional standard materials

**Table 1** Specifications of tested induction motor

Number of phases	3
Number of poles	4
Rated output	500 W
Voltage	200 V
Number of slots	Stator: 24, Rotor: 19
Stator slot shape	Open
Rotor slot shape	Semi closed
Skew	Non skewed
Connection of stator coil	Star

**Table 2** Material properties for tested core materials

	Density (kg/dm <sup>3</sup> )	W15/50 (W/kg)	B50 (T)	Hardness
50H-CL	7.80	3.48	1.74	127
50H-CH	7.80	4.33	1.75	114
50H470	7.70	3.45	1.70	155

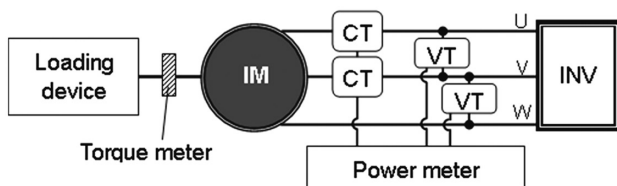


**Fig. 7** Composition of measurement system

temperature for the compensation of copper loss.

The motor properties were measured by a loading test driven by the inverter power source. The input power  $P_{in}$  (W) is calculated as the product of the voltage and the current measured by a power meter, and the output Power  $P_{out}$  (W) is calculated as the product of the rotation speed  $N$  (rpm) and the torque  $\tau$  (Nm) measured by a torque meter. The primary copper loss  $W_1$  (W) was compensated based on the stator core internal resistance  $R_1$  ( $\Omega$ ) measured at 20°C and the primary winding wire temperature  $t$  (°C) measured by the thermocouple.

The sum of the iron loss  $W_{iron}$  (W) and the secondary copper loss  $W_2$  (W) is obtained by subtracting the output, primary copper loss and mechanical loss  $W_m$  (W) from the input, as shown in the following formula.

$$W_{iron} + W_2 = P_{in} - P_{out} - W_1 - W_m \quad (6)$$

Further, the mechanical loss was measured separately and was 1.9 W at 1500 rpm.

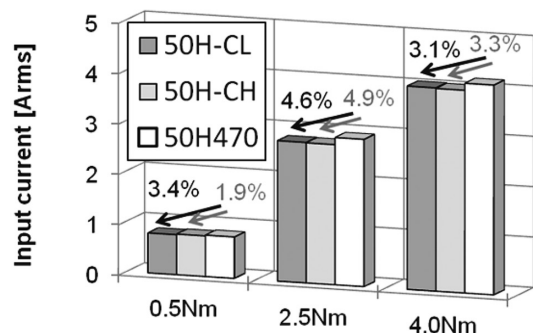
The test was conducted at three torque levels of 0.5 Nm (low torque), 2.5 Nm (rated torque) and 4.0 Nm (high torque), and at a constant rotation speed of 1500 rpm that corresponds to motor operation with no slip by a power frequency of 50 Hz. To maintain the constant output during the test, the excitation frequency was changed according to the torque levels.

**3.2 Result of experiment and study**

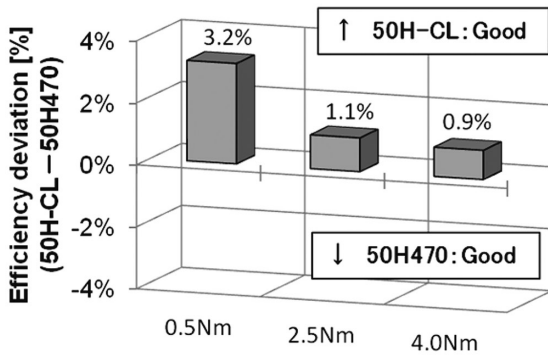
**Figure 8** shows the primary excitation currents at each torque condition. In comparison with the 50H470 core motor, exciting currents of the 50H-CL motor were 3.1–4.6% lower, which corresponds to a 6.9–9.0% improvement in primary copper loss. The exciting currents of 50H-CH were also 1.9–4.9% smaller than that of the 50H470 motor of the same torque condition, which means a 3.7–9.6% improvement of copper loss. These improvements correspond to their magnetizing properties shown in Fig. 6. Therefore, it can be stated that the newly developed 50H-CL and 50H-CH material improve motor efficiency by reducing the primary copper loss.

The efficiency improvement of the 50H-CL and 50H-CH motors compared to the 50H470 motor under each torque condition is shown in **Fig. 9**. The efficiency of the newly developed NO core motor is higher than that of 50H470 when the vertical axis value is positive. The result indicates that the 50H-CL core motor's efficiencies were higher from 0.9% to 3.2% than that of 50H470. The improvement is particularly significant in low torque as high as 3.2%. Furthermore, the 50H-CH core motor also exhibits the result of improvement of efficiency in the entire torque condition.

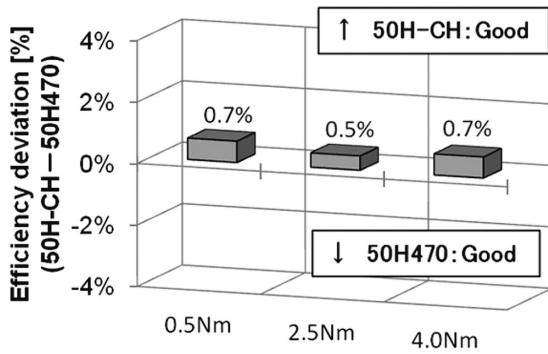
**Figure 10** shows details of the motor loss under various torque conditions. In the experiments, we used the same rotors and the ro-



**Fig. 8** Comparison of excitation currents in primary winding of test motors



(a) Efficiency improvement of motor using 50H-CL



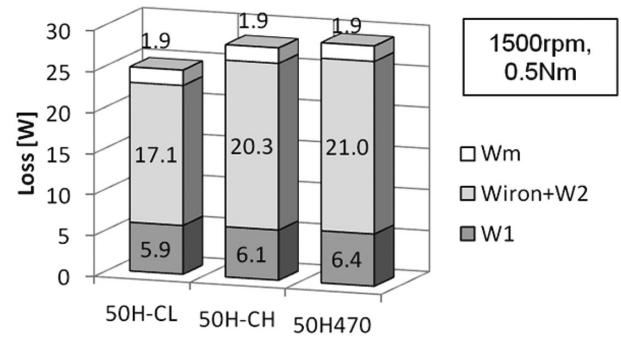
(b) Efficiency improvement of motor using 50H-CH

Fig. 9 Improvement of motor efficiency using the new material core at each operating condition

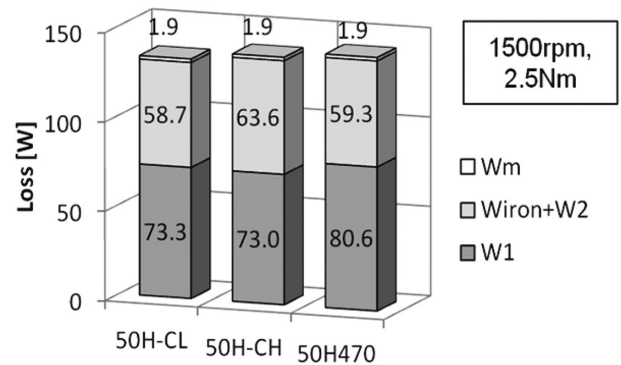
tation speed was fixed at 1500 rpm, and the mechanical loss  $W_m$  was assumed to be constant, 1.9W, under every torque condition. The total loss increases as the torque increases in all core motors. Both the primary copper loss ( $W_1$ ) and the sum of the iron loss and the secondary copper loss ( $W_{iron} + W_2$ ) increase, but the increase of the primary copper loss ( $W_1$ ) is significant. The ratio of the primary copper loss in the total loss is above 20% at the low torque condition (0.5Nm), but about 55% at the rated torque (2.5Nm) and high torque (4.0Nm). Accordingly, it is understood that the improvement of the motor efficiency at the rated and high torque conditions is mainly attributed to the reduction of the primary copper loss realized by the application of 50H-CL and 50H-CH with the high magnetic flux density characteristic.

At the low torque condition, the sum of the iron loss and the secondary copper loss ( $W_{iron} + W_2$ ) of the 50H-CL motor is significantly reduced. This improvement of the 50H-CL motor can be explained by its low iron loss and high induction property shown in Fig. 6 that reduced both motor iron loss and copper loss. In addition to that, the sum of iron loss and secondary copper loss in the 50H-CH motor also decreased compared to 50H470. This result implies that the high induction property reduced secondary copper loss in the rotor bar.

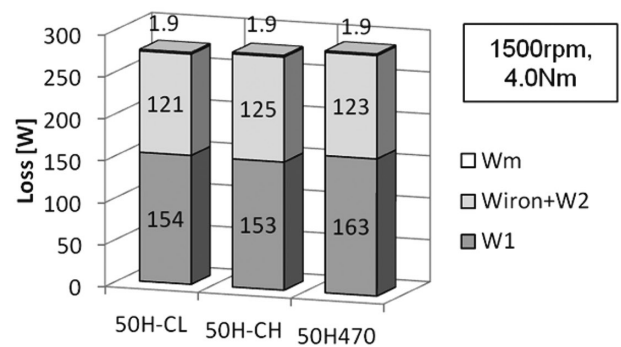
From the experimental results above, it can be concluded that the newly developed, non-oriented electrical steel sheets are suitable for improving the efficiency of induction motors and can contribute to an economical use of energy. It was confirmed that the effect of the reduction of copper loss is the major factor of the improvement, and in the case of the 50H-CL core motor, not only copper loss, but also the sum of iron loss and rotor copper loss were reduced, leading



(a) Motor losses (0.5 Nm / low torque)



(b) Motor losses (2.5 Nm / rated torque)



(c) Motor losses (4.0 Nm / maximum torque)

Fig. 10 Comparison of detail of motor loss of test inverter-fed induction motors

to further improvement.

#### 4. Conclusion

In this report, the calculation models for iron loss of inverter driven motors and the test results of induction motors employing newly developed, non-oriented electrical steel sheets were described as the basics of application technology of electrical steel sheets.

The scope of the application of motors is expected to be expanded as represented in the automotive industry area. Even under such circumstances, the non-oriented electrical steel sheet will continue to be the representative motor core material since it realizes excellent motor performances economically. Nippon steel & Sumitomo Metal Corporation will continue R&D of material and application technology of electrical steel sheets to contribute to advanced motor solutions.

### Acknowledgements

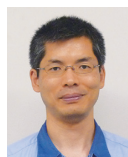
We wish to express our sincere appreciation to Mr. Shun Yoshida of Nippon Steel & Sumikin Technology Co., Ltd. for his contribution to this research and development study.

### References

- 1) Wajima, K., Fujiwara, K.: Evaluation of Iron Loss Calculation Models for NO Electrical Steel Sheets Excited by PWM Voltage of Distorted Flux Density. The Institute of Electrical Engineers of Japan Magnetics/Linear Drive Joint Study Report MAG-15-190/LD-15-100, 2015
- 2) Otome, D., Ozeki, Y., Miyagi, D., Nakano, M., Takahashi, N., Akatsu, K., Shiozaki, A., Kawabe, M.: Measurement of Iron Loss of Non-oriented Electrical Steel Sheet under PWM Inverter Excitation. The Institute of Electrical Engineers of Japan Magnetics Stationary Apparatus Rotary Machine Joint Study Report MAG-10-32/SA-10-32/RM-10-32, 2010
- 3) Odawara, S., Fujisaki, K., Matsuo, T.: Evaluation of Magnetizing Characteristic Considering Inverter Semiconductor Characteristic obtained by Numerical Analysis. The Institute of Electrical Engineers of Japan Magnetics LD-14-026, 2014
- 4) Domeki, H., Ishihara, Y., Kaido, C., Kawase, Y., Kitamura, S., Shimomura, T., Takahashi, N., Yamada, T., Yamazaki, K.: Investigation of Benchmark Model for Estimating Iron Loss in Rotating Machine. IEEE Trans. Magn. 40 (2), 794–797 (2004)
- 5) Kawase, Y., Yamaguchi, T., Sano, S., Igata, M., Ida, K., Yamagiwa, A.: 3-D Eddy Current Analysis in a Silicon Steel Sheet of an Interior Permanent Magnet Motor. IEEE Trans. Magn. 39 (3), 1448–1451 (2003)
- 6) Yamazaki, K., Fukushima, N.: Iron Loss Model for Rotating Machines Using Direct Eddy Current Analysis in Electrical Steel Sheets. IEEE Trans. Energy Conversion. 25 (3), 633–641 (2010)
- 7) Patent WO 2013-069754-A1. 2013
- 8) Nippon Steel & Sumitomo Metal Corporation Catalog, “Electrical Steel Sheets”. <http://www.nssmc.com/en/product/sheet/index.html>, 2013
- 9) Hirayama, R., Fujikura, M., Hori, K., Wajima, K.: Effect of Application of High Flux Density-Low Iron Loss Non-oriented Electrical Steel Sheets to Induction Motor. The Institute of Electrical Engineers of Japan Magnetics/Linear Drive Workshop MAG-14-215/LD-14-107, 2014



Kiyoshi WAJIMA  
Chief Researcher  
Instrumentation & Control Research Lab.  
Process Research Laboratories  
20-1 Shintomi, Futtsu City, Chiba Pref. 293-8511



Yasuo OHSUGI  
Senior Researcher  
Instrumentation & Control Research Lab.  
Process Research Laboratories



Ryu HIRAYAMA  
Chief Researcher, Dr.Eng.  
Instrumentation & Control Research Lab.  
Process Research Laboratories